nature communications

Article

https://doi.org/10.1038/s41467-025-57308-5

Circulating miR-126-3p is a mechanistic biomarker for knee osteoarthritis

Received: 31 May 2024

Accepted: 18 February 2025

Published online: 27 February 2025

Check for updates

Thomas G. Wilson[1], Madhu Baghel[1], Navdeep Kaur[1], Indrani Datta[2], Ian Loveless[2], Pratibha Potla[3], Devin Mendez[1], Logan Hansen[4], Kevin Baker[1], T. Sean Lynch[4], Vasilios Moutzouros[4], Jason Davis[4] & Shabana Amanda Ali[1,5]

Osteoarthritis is a major contributor to pain and disability worldwide, yet there are currently no validated soluble biomarkers or disease-modifying treatments. Given that microRNAs are promising mechanistic biomarkers that can be therapeutically targeted, in this study, we aimed to identify and prioritize reproducible circulating microRNAs associated with radiographic knee osteoarthritis. Across four independent cohorts, we find circulating miR-126-3p is elevated in knee osteoarthritis versus controls. Across six primary human knee osteoarthritis tissues, miR-126-3p is highest in subchondral bone, fat pad and synovium, and lowest in cartilage. Following both intravenous and intra-articular miR-126-3p mimic treatment in a surgical mouse model of knee osteoarthritis, we show reduced disease severity in males. In human knee osteoarthritis biospecimens, miR-126-3p mimic treatment reduces genes and markers associated with angiogenesis, as well as genes linked to osteogenesis, adipogenesis, and synovitis—processes secondary to angiogenesis. Our findings indicate that miR-126-3p is elevated in knee osteoarthritis and mitigates disease severity, supporting its potential as a biomarker and therapeutic target.

Osteoarthritis (OA) is a highly prevalent chronic joint disease that is estimated to reach up to one billion cases worldwide by 2050, with the knee being the most commonly affected joint[1]. Classically characterized by cartilage degradation[2], current understanding presents OA as far more complex, with knee OA involving multiple other joint tissues including subchondral bone, synovium, fat, ligaments and meniscus[3]. There are presently no approved disease-modifying OA drugs (DMOADs), with treatments limited to symptom management before surgical interventions are ultimately indicated[4]. As such, there is a need to identify minimally-invasive molecular biomarkers that can be used to detect OA when opportunities for preventative interventions still exist[4], and to better stratify individuals for recruitment to clinical trials evaluating DMOADs. MicroRNAs—small, non-coding RNA molecules—have emerged as a promising new class of biomarkers with the potential to meet this need[5].

As biomarkers, microRNAs have numerous advantages[5]. First, they are accessible via minimally-invasive liquid biopsies, as compared to more invasive synovial fluid or tissue biopsies[6]. Second, their short length (20–24 nucleotides) and frequent encapsulation in microvesicles make them resistant to enzymatic degradation and more stable than other molecules[6]. Third, microRNAs can be reliably quantified such that small changes can be linked to disease outcomes[7]. Fourth, microRNAs show tissue-specific expression patterns, making it possible to map their role in complex diseases[8]. Fifth, microRNAs are

[1]Bone and Joint Center, Henry Ford Health + Michigan State University Health Sciences, Detroit, MI, USA. [2]Center for Bioinformatics, Henry Ford Health + Michigan State University Health Sciences, Detroit, MI, USA. [3]Schroeder Arthritis Institute, University Health Network, Toronto, ON, Canada. [4]Department of Orthopedic Surgery, Henry Ford Health, Detroit, MI, USA. [5]Center for Molecular Medicine and Genetics, Wayne State University, Detroit, MI, USA.
e-mail: sali14@hfhs.org

known drivers of OA pathology, and their expression precedes phenotypic changes in tissues[9]. MicroRNAs are already in clinical use as biomarkers for musculoskeletal disorders such as osteoporosis[10]. Despite the potential of circulating microRNAs to serve as biomarkers of knee OA, a lack of reproducibility across microRNA profiling studies continues to be a hurdle to clinical translation.

Beyond biomarkers, microRNAs are important epigenetic factors with mechanistic roles in musculoskeletal health and disease, and therefore represent promising therapeutic targets[11]. Produced in cells throughout the body, microRNAs are encoded in host genes and transcribed as primary stem loop structures (pri-microRNAs) that are processed by Drosha enzymes into precursor molecules (pre-microRNAs), then by Dicer enzymes into mature microRNAs[12]. Primarily functioning to inhibit gene target expression through direct seed sequence binding, microRNAs can act locally in the producing cell, or distally in target cells[13,14]. MicroRNAs are known to impact a variety of disease processes in OA, including inflammation, extracellular matrix dysregulation, cell death and proliferation[9,11,15]. A notable therapeutic advantage of microRNAs, they can be readily modulated with small molecules in a targeted manner[16,17].

The gold standard for microRNA discovery is sequencing, which enables sensitive, specific and high-throughput quantification of microRNAs in a given biospecimen[18]. To date there are only two published microRNA-sequencing studies that have evaluated circulating microRNAs between individuals with and without OA[19,20]. The first study reported no significant differences in OA plasma extracellular vesicle microRNAs[19], and the second study reported three differentially expressed (DE) microRNAs in OA serum, none of which were validated in subsequent experiments[20].

In the current study, we leverage a customized microRNA-sequencing analysis pipeline[18] to re-analyze these two datasets in search of reproducible circulating microRNAs associated with knee OA, and prioritize miR-126-3p. We then characterize miR-126-3p levels and potential mechanisms of action using both primary human knee OA tissues and a surgical mouse model of knee OA. Overall, our findings suggest miR-126-3p becomes elevated during knee OA as a mechanism to mitigate disease processes and attenuate OA severity.

Results

Circulating miR-126-3p is elevated in knee OA versus non-OA in independent cohorts

Taking an unbiased approach to identifying circulating microRNAs associated with knee OA versus non-OA, we leveraged two existing microRNA-sequencing datasets. These studies comprised Cohort 1 from Norway[19] and Cohort 2 from France[20] that previously reported zero and three DE microRNAs, respectively, none of which were subsequently validated. Leveraging the raw data from these studies, we performed secondary analysis using a customized microRNA-sequencing pipeline[18] developed in previous studies[7,21] (Fig. 1A). Specifically, we first defined knee OA based on Kellgren-Lawrence (KL) radiographic grade[22], considering KL 3 or 4 as knee OA and KL 0 as non-OA controls. These definitions were more stringent than those used in the original analyses, which for example, included KL 1 for controls[20]. Next, we performed a two-step read alignment, utilizing both miRBase v22.1 and the human reference genome (GRCh38), which captured additional microRNA reads that would otherwise not be aligned using a single reference database[18]. We then performed filtering to select microRNAs with a minimum of ten counts-per-million (CPM) in two or more samples and normalized the counts to total aligned sequences, consistent with previous studies[7,21]. Differential expression analysis identified 23 microRNAs in OA versus non-OA individuals from Cohort 1 and 82 microRNAs from Cohort 2 at $p < 0.1$, with three DE microRNAs in common: miR-126-3p, miR-30c-2-3p, and miR-144-5p (Fig. 1A). Amongst these three microRNAs, miR-126-3p exhibited the highest CPM (i.e., abundance), showed a consistent positive fold-change in OA versus non-OA, and had the lowest p-value in both cohorts (Fig. 1B). This data-driven discovery of circulating miR-126-3p in radiographic knee OA led us to prioritize it for further characterization.

Circulating miR-126-3p can accurately distinguish radiographic knee OA

To investigate miR-126-3p as a candidate biomarker for radiographic knee OA, we sought to define the patient population in which it is elevated using our Henry Ford Health (HFH) OA Cohort, a collection of primary human biofluids, tissues and clinicodemographic data from $N = 145$ consenting patients undergoing knee or hip arthroplasty or arthroscopy (Supplemental Table 1). After stratifying by joint (knee or hip) and KL grade, we measured miR-126-3p, miR-30c-2-3p, and miR-144-5p in plasma by real-time polymerase chain reaction (RT-PCR). While no significant differences were found for miR-30c-2-3p or miR-144-5p (Supplemental Fig. 1), we found miR-126-3p was significantly elevated in KL ≥ 2 knee OA versus non-OA (controls with no evidence of OA; Fig. 2A). Notably, there was no increase in miR-126-3p in KL ≥ 3 hip OA, and levels between KL 2, 3, and 4 knee OA were not different at $p < 0.05$ (Fig. 2A). Since both microRNA levels[23] and OA outcomes[24] are influenced by age, sex and body mass index (BMI), we next assessed the association of these variables with plasma miR-126-3p levels within knee OA patients using multiple linear regression analysis and found no association, whereas KL grade showed a significant positive association (Fig. 2B). In support of this, a previous study from Mexico reported increased levels of miR-126 in plasma from individuals with KL 2 and 3 knee OA versus controls[25]. We combined these findings with our own in a meta-analysis which showed miR-126-3p is consistently elevated in radiographic knee OA compared to non-OA controls across four independent cohorts, with a pooled effect size of logFC 0.55 ($p = 0.002$; Supplemental Fig. 2).

To assess the extent to which plasma miR-126-3p could be used to distinguish radiographic knee OA, we performed area under the receiver operating characteristic curve (AUC) analysis and found models including miR-126-3p had 'excellent' accuracy in distinguishing KL ≥ 2 knee OA from hip OA (AUC = 0.91, sensitivity = 0.91, specificity = 0.71; Fig. 2C). This comparison was chosen since the knee OA and hip OA groups exhibit more similar clinicodemographic composition than the knee OA and non-OA groups (Supplemental Table 1), and hip OA miR-126-3p levels are similar to those in non-OA individuals (Fig. 2A). Based on its reproducibility across cohorts and accuracy in distinguishing KL ≥ 2 knee OA, our findings suggest circulating miR-126-3p is a promising candidate biomarker for radiographic knee OA.

Circulating miR-126-3p originates from knee OA fat pad

To assess the specificity of circulating miR-126-3p to knee OA, we measured mature miR-126-3p by RT-PCR in subchondral bone, infrapatellar fat pad (fat pad), synovium, anterior cruciate ligament (ligament), meniscus and articular cartilage from individuals with OA undergoing total knee arthroplasty. First, we found mature miR-126-3p levels were highest in subchondral bone, fat pad and synovium as compared to cartilage, the tissue with the lowest average levels (Fig. 3A). Second, we compared miR-126-3p tissue levels to plasma levels in matched samples and found significant positive correlations for subchondral bone, fat pad and synovium only (Fig. 3B). Third, we evaluated active production (transcription and processing) of miR-126-3p by measuring pri-mir-126, *DROSHA*, pre-mir-126 and *DICER1* (Fig. 3C), each of which showed the highest average expression in fat pad compared to cartilage (Fig. 3D–G). Despite the high levels of mature miR-126-3p observed in subchondral bone (Fig. 3A), we saw relatively low active production of miR-126-3p in this tissue, as compared to cartilage (Fig. 3D–G). Based on these findings, we hypothesized fat pad is a putative source of circulating miR-126-3p, while subchondral bone is a putative sink. We

https://doi.org/10.1038/s41467-025-57308-5

next measured secretion of mature miR-126-3p over time by each of the six knee OA tissues ex vivo. Conditioned media from tissue explants were collected and replaced after 24, 48, and 72 hours of culture, and miR-126-3p measured by RT-PCR (Fig. 3H). While cartilage, meniscus and ligament showed a steady rate of miR-126-3p secretion in each 24-hour period, synovium and fat pad showed an acceleration and subchondral bone a deceleration (Fig. 3I). Taken together these data indicate fat pad is most actively producing (Fig. 3D–G) and secreting (Fig. 3I) miR-126-3p, while subchondral bone is not. These findings link circulating miR-126-3p to knee OA tissues, with fat pad as a putative source tissue, and subchondral bone as a putative sink.

A

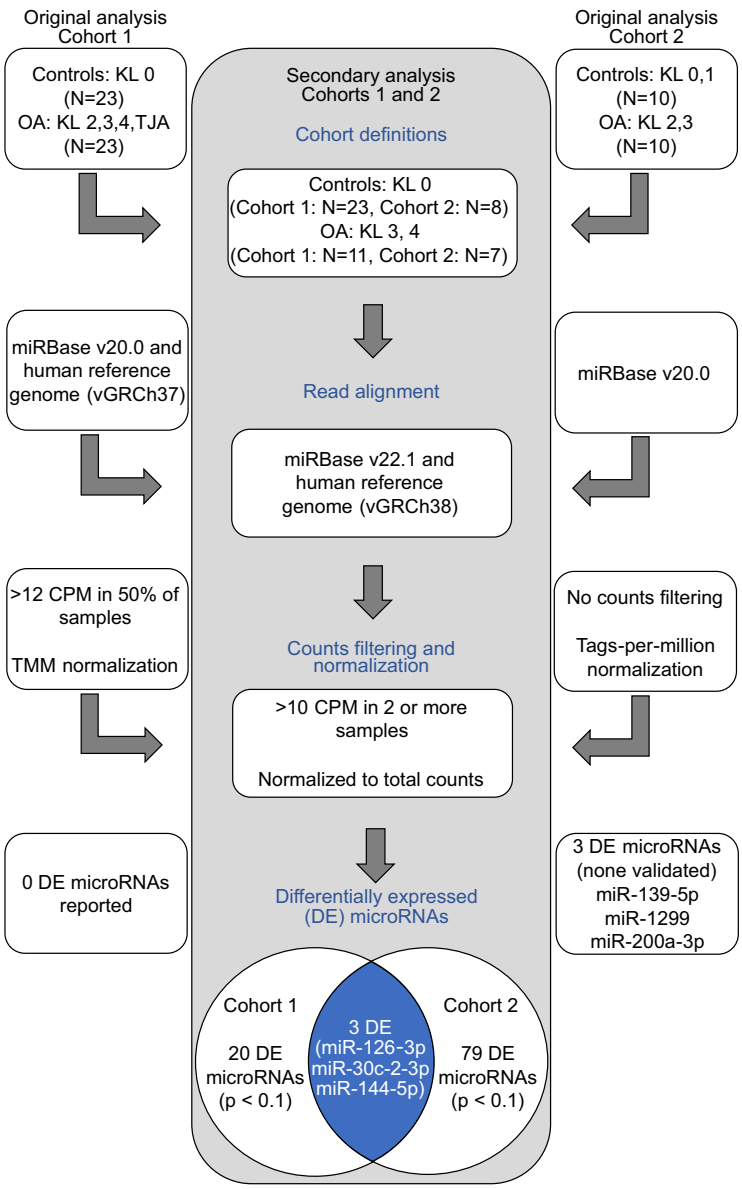

B

	Cohort 1			Cohort 2		
microRNA	logCPM	logFC	p-value	logCPM	logFC	p-value
miR-126-3p	16.3	0.23	0.022	13.8	0.53	0.006
miR-30c-2-3p	3.7	0.77	0.024	2.8	0.97	0.065
miR-144-5p	6.5	0.51	0.026	7.1	-0.56	0.058

Fig. 1 | Circulating miR-126-3p is elevated in knee OA versus non-OA in two independent microRNA-sequencing datasets. A Overview of secondary analysis of two microRNA-sequencing datasets analyzed according to a customized analysis pipeline[18]. Left and right columns show details from the original analyses of Cohort 1[19] and Cohort 2[20], respectively, while the center column highlights our modifications and results. KL Kellgren-Lawrence grade, TJA total joint arthroplasty, CPM counts-per-million, TMM trimmed mean of *m*-values. **B** Three differentially expressed (DE) microRNAs in knee OA versus non-OA were common in both datasets. LogCPM $\log_2$ counts-per-million, logFC $\log_2$ fold-change, unadjusted *p*-values determined by two-sided quasi-likelihood *F*-test.

https://doi.org/10.1038/s41467-025-57308-5

A

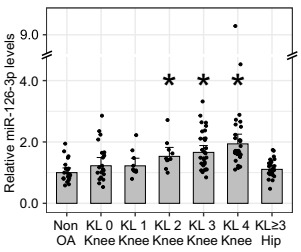

B

Variable	Unstandardized Coefficient (95% CI)	p-value
Age (years)	-0.001 (-0.13 – 0.10)	0.802
Sex	-0.079 (-0.311 – 0.153)	0.500
BMI (kg/m^2)	-0.009 (-0.029 – 0.011)	0.367
KL grade	0.193 (0.058 – 0.328)	0.006

C

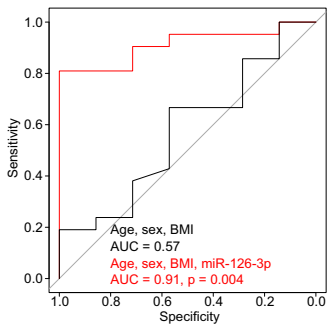

Fig. 2 | Circulating miR-126-3p distinguishes radiographic knee OA with excellent accuracy. A Relative miR-126-3p levels in plasma samples collected from the Henry Ford Health (HFH) OA Cohort, stratified by joint and KL grade (Non-OA: $n = 20$, KL 0 Knee: $n = 20$, KL 1 Knee: $n = 10$, KL 2 Knee: $n = 10$, KL 3 Knee: $n = 30$, KL 4 Knee: $n = 30$, KL ≥ 3 Hip: $n = 25$ biological replicates). Values represent fold-change relative to the mean value of non-OA controls. Bars represent mean fold-change ± 95% confidence interval, statistical significance determined by two-sided Mann–Whitney *U* test with Benjamini-Hochberg correction, $^*p < 0.05$ versus non-OA. **B** Multiple linear regression analysis assessing the association of each variable with plasma miR-126-3p levels in knee OA. BMI body mass index, 95% CI 95% confidence interval. Statistical significance for regression coefficients determined by two-sided *t*-tests. **C** Receiver operating characteristic curve analysis of a test cohort of HFH OA plasma samples displaying the accuracy of two models in distinguishing radiographic knee and hip OA. Black line represents a model consisting of age, sex and BMI; red line represents a model consisting of age, sex, BMI and relative miR-126-3p plasma levels. AUC area under the receiver operating characteristic curve, $p =$ versus age, sex, BMI only, statistical significance determined by two-sided DeLong's test. Source data are provided as a Source Data file. *P*-values: **A** $p = 0.214$ (KL 0 Knee), $p = 0.214$ (KL 1 Knee), $p = 0.010$ (KL 2 Knee), $p = 0.000$ (KL 3 Knee), $p = 0.000$ (KL 4 Knee), $p = 0.244$ (KL ≥ 3 Hip).

miR-126-3p attenuates the severity of knee OA in a surgical mouse model

To investigate the effect of miR-126-3p on knee OA in vivo, we leveraged an established surgical mouse model comprising partial medial meniscectomy (PMX)[26,27] or sham surgery (Fig. 4A). We compared miR-126-3p in plasma from PMX versus sham mice at four weeks post-surgery (16 weeks) and found an average 2.3-fold increase relative to pre-surgical levels (12 weeks; Fig. 4B). This suggests knee OA is sufficient to induce elevated circulating miR-126-3p and supports the use of the PMX model for evaluating effects of miR-126-3p modulation on knee OA. Beginning four weeks post-operatively to approximate moderate knee OA[27] (i.e., KL ≥ 2, when circulating miR-126-3p becomes elevated in humans; Fig. 2A), weekly tail vein injections of 5 μg miR-126-3p mimic, miR-126-3p inhibitor or negative control were delivered. After sacrifice (20 weeks), we performed OARSI histopathology scoring on Safranin-O stained sections of knee joints, where higher values reflect more cartilage damage[28]. We found miR-126-3p mimic treatment reduced OARSI score in PMX mice as compared to both miR-126-3p inhibitor and negative control treatments, reflecting less cartilage damage (Fig. 4C, D). We also performed synovitis scoring (where higher values reflect more synovitis[29]) and similarly found lower scores with miR-126-3p mimic in PMX mice as compared to miR-126-3p inhibitor, reflecting only slight synovitis (Fig. 4E, F). Higher magnification images are provided in Supplemental Fig. 3 to illustrate changes in cartilage and synovial lining thickness. We next repeated this experiment as depicted in Fig. 4A, but delivered miR-126-3p mimic or negative control via intra-articular (IA) injection. We again observed less cartilage damage and synovitis in mimic-treated mice compared to controls (Supplemental Fig. 4). There was no notable effect of these treatments in the sham groups for either outcome. Taken together, these data suggest that both systemic and local delivery of miR-126-3p improves knee OA outcomes in a preclinical model.

miR-126-3p has anti-angiogenic effects in knee OA

Based on previous literature in vascular systems, miR-126-3p is expressed primarily by endothelial cells and functions to regulate angiogenesis[30,31]. Consistent with this, we observed miR-126-3p primarily in regions where endothelial cells line vessels in each of subchondral bone, fat pad and synovium (Supplemental Fig. 5). We therefore identified validated direct gene targets of miR-126-3p associated with angiogenesis from the literature[30,32–38] for assessment in the context of knee OA. Using RT-PCR, we first confirmed effective modulation of miR-126-3p in primary human knee OA subchondral bone, fat pad and synovium tissue explants following transfection with 100 nM miR-126-3p mimic versus control (Supplemental Fig. 6). We next measured changes in expression of sprouty related EVH1 domain containing 1 (*SPRED1*), which is reported to inhibit angiogenesis[30,32], as well as a disintegrin and metalloproteinase domain 9 (*ADAM9*)[33], insulin receptor substrate 1 (*IRS1*)[34] and vascular endothelial growth factor A (*VEGFA*)[38], which are reported to enhance angiogenesis[35–38]. As expected of the inhibitory effect of microRNAs on their direct gene targets, we found reduced expression of all four genes with miR-126-3p mimic, except *IRS1* in synovium ($p = 0.18$) and *VEGFA* in subchondral bone ($p = 0.13$; Fig. 5A–D). To assess the net effect of miR-126-3p on angiogenesis, we used both in vivo and in vitro models. In our mouse model, endothelial cells marked by CD31 showed an increase in PMX versus sham mice, consistent with literature reporting angiogenesis is increased during knee OA[39] (Fig. 4G). Looking at synovium and subchondral bone, miR-126-3p mimic groups showed reduced CD31 staining compared to both miR-126-3p inhibitor and negative control groups (Fig. 4G). From primary human tissues, isolated endothelial cells transfected with miR-126-3p mimic showed reduced ability to form 3D tube structures compared to control (Fig. 5E). Looking at synovium and subchondral bone, multiple metrics associated with angiogenesis showed a decrease with miR-126-3p mimic versus control (Fig. 5F, G). Though similar trends were found in human fat pad, these were not statistically significant (Supplemental Fig. 7), and mouse fat pad was not visible in coronal sections. Overall, these findings suggest miR-126-3p reduces angiogenesis in knee OA.

Since angiogenesis is associated with knee OA outcomes[39], we next investigated OA processes in each of subchondral bone, fat pad and synovium that have been reported as secondary to angiogenesis[39,40]. Following treatment with miR-126-3p mimic, we found decreased gene expression of osteocalcin (*OCN*), osterix (*OSX*) and runt-related transcription factor 2 (*RUNX2*) in subchondral bone (Fig. 5H); decreased leptin (*LEP*), adiponectin (*ADIPOQ*) and a trend towards decreased CCAAT/enhancer-binding protein-alpha (*CEBPA*; $p = 0.11$) in fat pad (Fig. 5I); and decreased interleukin 1 beta (*IL1b*),

https://doi.org/10.1038/s41467-025-57308-5

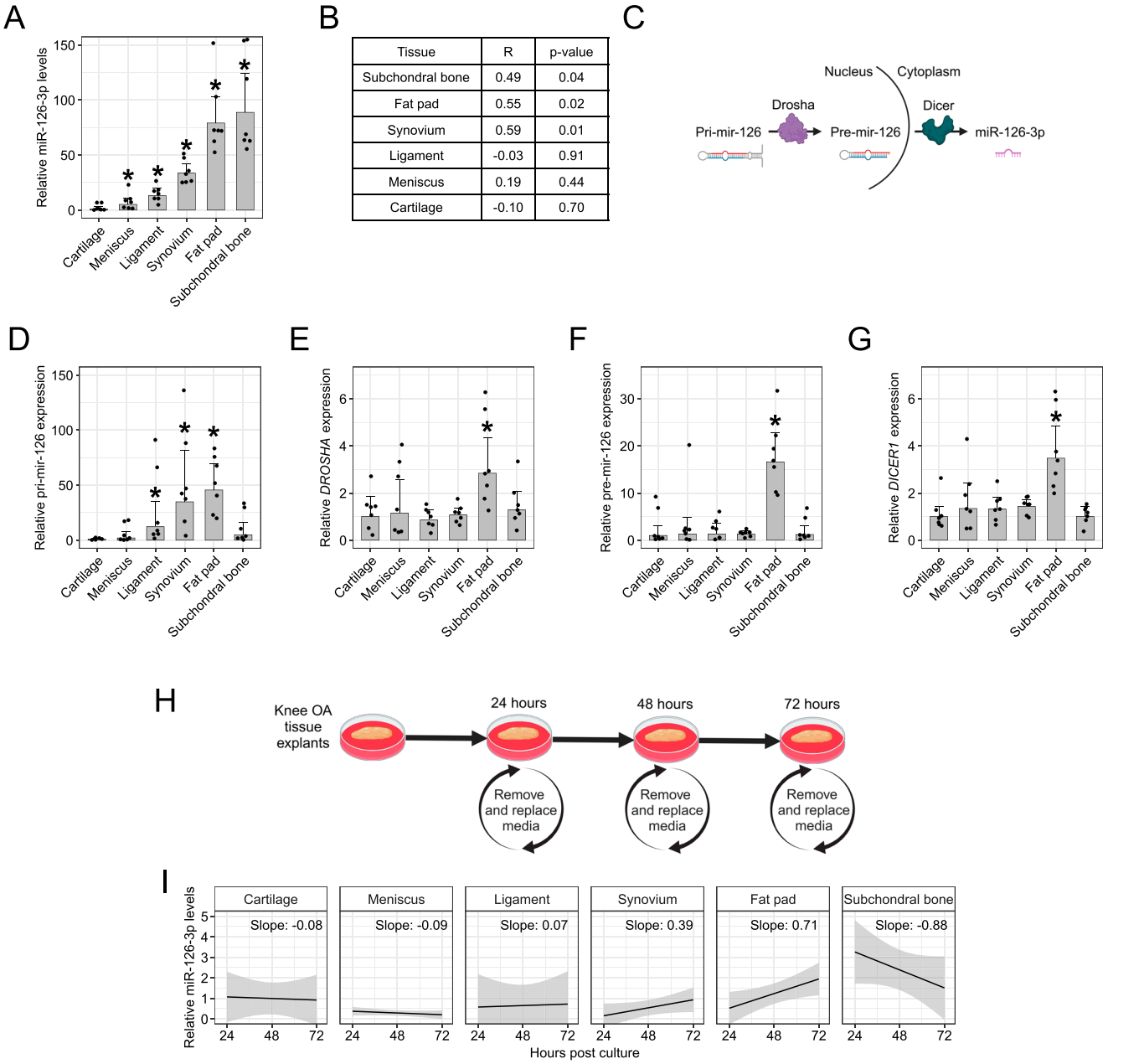

Tissue	R	p-value
Subchondral bone	0.49	0.04
Fat pad	0.55	0.02
Synovium	0.59	0.01
Ligament	-0.03	0.91
Meniscus	0.19	0.44
Cartilage	-0.10	0.70

Fig. 3 | Knee OA fat pad is a putative source of miR-126-3p and subchondral bone a putative sink. A Mature miR-126-3p levels in six primary human knee OA tissues ($n = 7$ biological replicates). Data represent fold-change values relative to mean cartilage expression. Bars represent mean fold-change ± 95% confidence interval. Statistical significance determined by one-way ANOVA with two-sided Dunnett's post hoc test, $^*p < 0.05$ versus cartilage. **B** Pearson correlation analysis between miR-126-3p levels in matched tissue and plasma samples from knee OA individuals ($n = 18$ biological replicates). *R* = correlation coefficient. *P*-values determined by two-sided *t*-test for Pearson correlation. **C** Overview of miR-126-3p production showing key factors measured in six primary human knee OA tissues, including (**D**) pri-mir-126, (**E**) *DROSHA*, (**F**) pre-mir-126 and (**G**) *DICER1*. Created in BioRender. Wilson, T. (2025) https://BioRender.com/q28v824. **D**–**G** Data represent fold-change values relative to mean cartilage expression ($n = 7$ biological replicates). Bars represent mean ± 95% confidence interval. Statistical significance determined by one-way ANOVA with two-sided Dunnett's post hoc test, $^*p < 0.05$ versus cartilage. **H** Overview of experimental design for assessing miR-126-3p secretion over time. Created in BioRender. Wilson, T. (2025) https://BioRender.com/b86a692. **I** Secretion of miR-126-3p from knee OA tissues. Data fitted from miR-126-3p fold-change values relative to a reference microRNA (miR-24-3p) at each timepoint [$n = 4$ biological replicates (cartilage, meniscus, ligament), $n = 7$ biological replicates (synovium, fat pad, subchondral bone)], black line = fitted linear model, grey region = 95% confidence interval. Source data are provided as a Source Data file. *P*-values: **A** $p = 0.003$ (meniscus), $p = 0.000$ (ligament), $p = 0.000$ (synovium), $p = 0.000$ (fat pad), $p = 0.000$ (subchondral bone). **D** $p = 0.770$ (meniscus), $p = 0.005$ (ligament), $p = 0.000$ (synovium), $p = 0.000$ (fat pad), $p = 0.118$ (subchondral bone). **E** $p = 0.996$ (meniscus), $p = 0.992$ (ligament), $p = 1.000$ (synovium), $p = 0.040$ (fat pad), $p = 0.948$ (subchondral bone). **F** $p = 0.991$ (meniscus), $p = 0.993$ (ligament), $p = 0.994$ (synovium), $p = 0.001$ (fat pad), $p = 0.998$ (subchondral bone). **G** $p = 0.721$ (meniscus), $p = 0.771$ (ligament), $p = 0.560$ (synovium), $p = 0.000$ (fat pad), $p = 1.000$ (subchondral bone).

interleukin 6 (*IL6*) and tumor necrosis factor alpha (*TNFa*) in synovium (Fig. 5J). Since none of these genes contain a miR-126-3p seed sequence binding site, these findings suggest miR-126-3p may mitigate knee OA by directly reducing angiogenesis and indirectly attenuating the osteogenesis associated with sclerosis and osteophytosis[41], the adipogenesis associated with metabolic and signaling perturbations[42], and the inflammatory response associated with synovitis[43] (Fig. 6).

https://doi.org/10.1038/s41467-025-57308-5

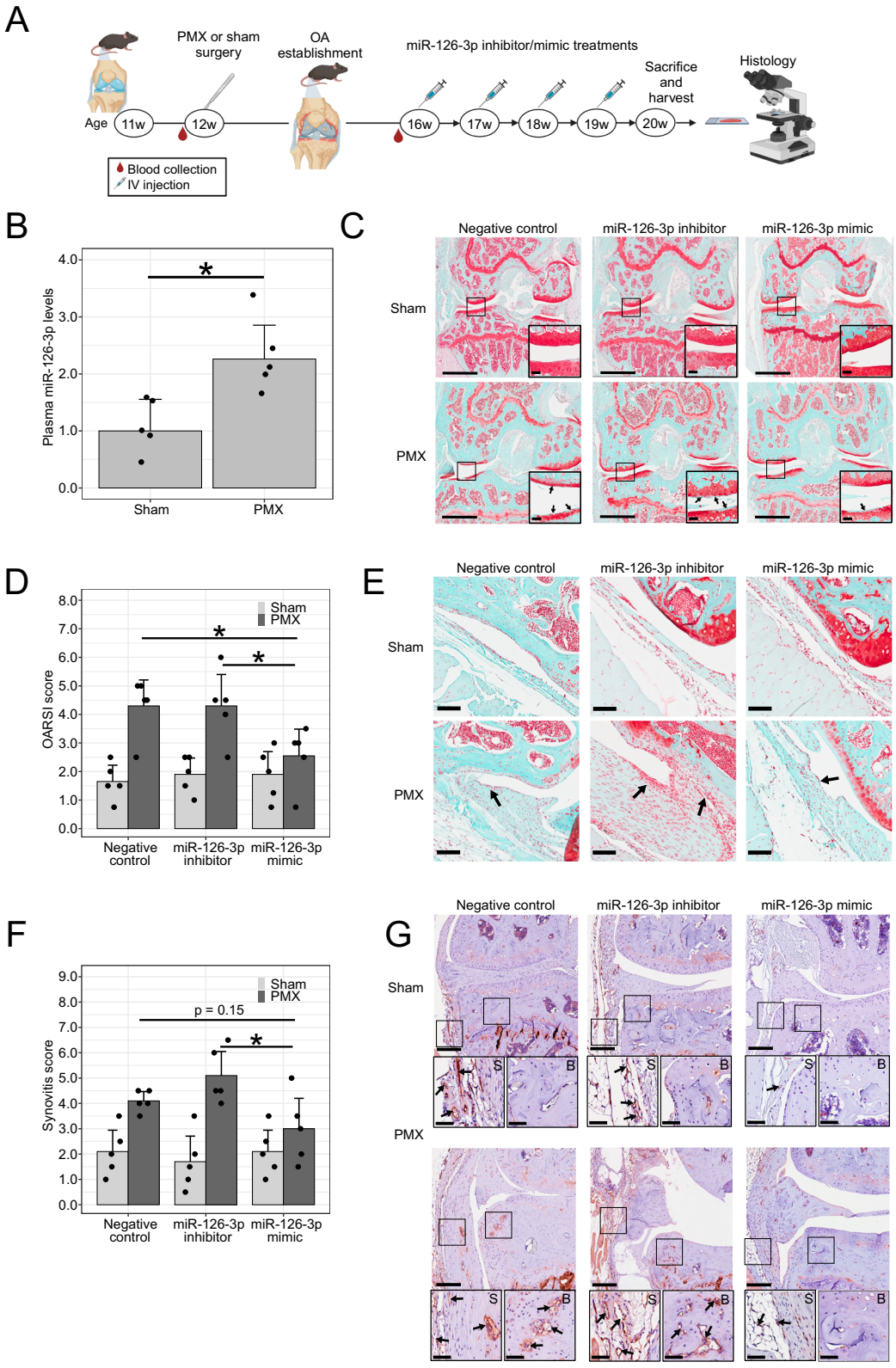

Discussion

The objective of this study was to identify reproducible microRNAs as candidate mechanistic biomarkers for knee OA. With a data-driven approach, we leveraged a customized pipeline for microRNA-sequencing analysis[18] and two previously published datasets[19,20] to prioritize circulating microRNAs in knee OA. We discovered and characterized miR-126-3p as a putative mechanistic biomarker for KL ≥ 2 knee OA, a stage considered to be moderate OA[44], when opportunities for intervention to prevent or delay progression to end-stage disease still exist. This type of minimally-invasive and cost-effective biomarker could be useful for recruitment of more homogeneous patient populations to clinical trials testing novel DMOADs or

Fig. 4 | miR-126-3p improves outcomes in a surgical mouse model of knee OA. **A** Overview of experimental design for mouse surgery, treatments and endpoints. w weeks-old, PMX partial medial meniscectomy, IV intravenous. Created in BioRender. Wilson, T. (2025) https://BioRender.com/x45j911. **B** Plasma miR-126-3p levels in PMX versus sham mice at 4-weeks post-surgery (16w) relative to pre-surgery (12w) in negative control groups ($n = 5$ biological replicates). Bars represent mean ± 95% confidence interval, $^*p < 0.05$. **C** Representative coronal sections of mouse operated knee stained with Safranin-O. Scale bars = 1 mm. Insets show magnified regions (scale bars = 100 μm, arrows = examples of cartilage damage). **D** OARSI scoring by blinded observers of PMX and sham mice following miR-126-3p treatments ($n = 5$ biological replicates). Bars represent mean maximal quadrant score ± 95% confidence interval, $^*p < 0.05$. **E** Representative sections of synovium from mouse operated knee. Scale bars = 100 μm, arrows = examples of synovitis. **F** Krenn synovitis scoring by blinded observers ($n = 5$ biological replicates). Bars represent mean synovitis score ± 95% confidence interval, $^*p < 0.05$. **G** Representative sections of mouse operated knee stained for cluster of differentiation (CD31). Scale bars = 200 μm. Insets show magnified regions of synovium ("S") and subchondral bone ("B"); scale bars = 50 μm, arrows = examples of CD31 staining corresponding to endothelial cells. Source data are provided as a Source Data file. All statistical significance determined by unadjusted two-sided Student's *t*-test. *P*-values: **B** $p = 0.018$. **D** $p = 0.030$ (miR-126-3p mimic vs. negative control), $p = 0.046$ (miR-126-3p mimic vs. miR-126-3p inhibitor). **F** $p = 0.150$ (miR-126-3p mimic vs. negative control), $p = 0.029$ (miR-126-3p mimic vs. miR-126-3p inhibitor).

other OA therapies, including those focused on mitigating aberrant angiogenesis[45,46]. Together with our HFH OA Cohort in the USA, we identified four independent datasets from four countries (including Norway[19], France[20], and Mexico[25]) consistently showing elevation of miR-126-3p in knee OA versus non-OA controls. Moreover, with respect to biofluids, two cohorts measured miR-126-3p in plasma[25], one in serum[20] and one in plasma extracellular vesicles[19]; with respect to assays, two cohorts used sequencing[19,20], one used RT-PCR array[25] and one used RT-PCR. This diversity in biofluids and assays supports the robustness of our finding and points to the clinical utility of miR-126-3p as a biomarker wherein it could be measured in any readily accessible blood fraction using a common RT-PCR assay. To note limitations, low sample sizes limited statistical significance in the sequencing data after false-discovery-rate correction[47], and classification models were built using hip OA as a comparator to minimize confounding variables. Furthermore, assessment of the diagnostic accuracy of miR-126-3p is still needed, in compliance with established guidelines[48]. Looking at the broader literature, inclusion of miR-126-3p into composite biomarker profiles has proven useful for diseases like cancer[49], suggesting the accuracy of our miR-126-3p model (AUC = 0.91) could be strengthened by including other emerging sensitive and specific biomarkers for knee OA (e.g., cartilage acidic protein 1[5]) to improve identification of individuals with knee OA.

MicroRNAs are known to play important regulatory roles in biological processes that impact disease[9,11]. Since microRNAs typically function to inhibit expression of their direct gene targets in a tissue-dependent manner[8], we again undertook a data-driven approach to prioritizing knee OA tissues for further characterization of miR-126-3p. This proved to be an advantage over OA studies that focus on cartilage a priori, as our profiling of six different knee tissues revealed roles for subchondral bone, fat pad and synovium, and relatively low levels of miR-126-3p in cartilage. A previous study exploring miR-126-3p in cartilage reported reduced levels in OA versus control and in old versus young cartilage[50], whereas we found increased miR-126-3p levels in OA versus control plasma, and no association with age. Since we did not identify correlations between plasma and cartilage miR-126-3p levels in matched samples, the mechanisms governing miR-126-3p in cartilage may be distinct, particularly since cartilage is avascular and miR-126-3p is primarily expressed by endothelial cells[30,31,51]. Our findings support the view of OA as a disease of the whole joint and put forth a role for tissue crosstalk with fat pad and synovium as potential source tissues of miR-126-3p and subchondral bone as a potential sink tissue. While our investigation into source and sink tissues was not exhaustive across the body, and more definitive experiments are required (e.g., tracing labeled microRNAs from source to sink[52]), data from our preclinical model suggest moderate knee OA is sufficient to produce elevated circulating levels of miR-126-3p. In support of fat pad as a putative source tissue, adipose-derived microRNAs are known to be a source of circulating microRNAs that can regulate genes in other tissues[14]. In the context of knee OA, fat pad appears to be the most active tissue in terms of microRNA processing overall, based on its higher levels of *DROSHA* and *DICER1*. Our data indicate fat pad is responsible at least in part for driving elevated circulating levels of miR-126-3p in knee OA, and the purpose of this may be to target subchondral bone, which shows high levels of mature miR-126-3p, but low production. In support of distal source tissues targeting subchondral bone as a sink tissue, synovium-derived miR-126-3p-rich exosomes have been shown to attenuate subchondral bone phenotypes in an OA rat model[53]. Notably, we found miR-126-3p in synovium conditioned media increased over time, suggesting it may be acting as a secondary source (given its lower levels) of miR-126-3p. It remains unclear why subchondral bone does not produce miR-126-3p locally, particularly given the importance of vasculature in regulating bone formation, resorption and inflammatory processes[54–56]. This points to the need for additional research to elucidate mechanisms of miR-126-3p specifically in knee OA subchondral bone, fat pad and synovium.

With evidence to support elevated circulating levels of miR-126-3p originating at least in part from knee OA tissues, we next used a preclinical model to investigate effects on knee OA outcomes and found systemic miR-126-3p mimic reduced cartilage damage and synovitis. Though we were unable to confirm modulation of miR-126-3p levels directly in the knee joint, likely owing to the short half-life of microRNA mimics[57], we were able to show similar phenotypic effects on knee OA following intra-articular delivery of miR-126-3p mimic. These findings are consistent with the only other study exploring miR-126-3p in knee OA in vivo, reporting reduced osteophyte formation, cartilage degeneration and synovial inflammation in a surgical rat model following intra-articular delivery of exosomes carrying miR-126-3p[53]. Taken together this suggests that miR-126-3p has a pro-resolving effect in knee OA and may become elevated at KL ≥ 2 to mitigate disease processes. Though additional experiments are required to investigate the therapeutic potential of miR-126-3p, these data suggest there may be value in administering it earlier in the disease course (KL < 2) or at higher levels later in the disease course to improve knee OA outcomes. MicroRNAs are known to be promising therapeutic targets, with several clinical trials testing microRNA mimic-based treatments for conditions such as keloid disorders[58], mesothelioma[59] and advanced solid tumors[60]. Efforts are ongoing to overcome obstacles limiting microRNA-based therapies, including optimizing effective dosing and delivery methods, and minimizing unwanted off-target effects[16,61].

In terms of mechanisms through which miR-126-3p may be acting in knee OA, our data point to angiogenesis. Previous studies show miR-126-3p can have both pro- and anti-angiogenic effects in a context-dependent manner[30,62]. In cancer and cardiovascular disease, miR-126-3p is known to regulate angiogenesis via direct targeting of *SPRED1*, *IRS1*, *ADAM9* and *VEGFA*, among others[34,37,38,63]. In OA, endothelial cell populations are enriched[56] and angiogenesis is increased in multiple tissues including synovium, fat pad and subchondral bone[39,64]. This is generally thought to be detrimental by promoting inflammation, pain and structural damage[39,65]. We observed anti-angiogenic effects of miR-126-3p both in vivo and in vitro, which are consistent with an overall pro-resolving role in knee OA. The reduced gene expression in markers of osteogenesis, adipogenesis and synovitis we observed were through indirect mechanisms (i.e., not via direct miR-126-3p seed

https://doi.org/10.1038/s41467-025-57308-5

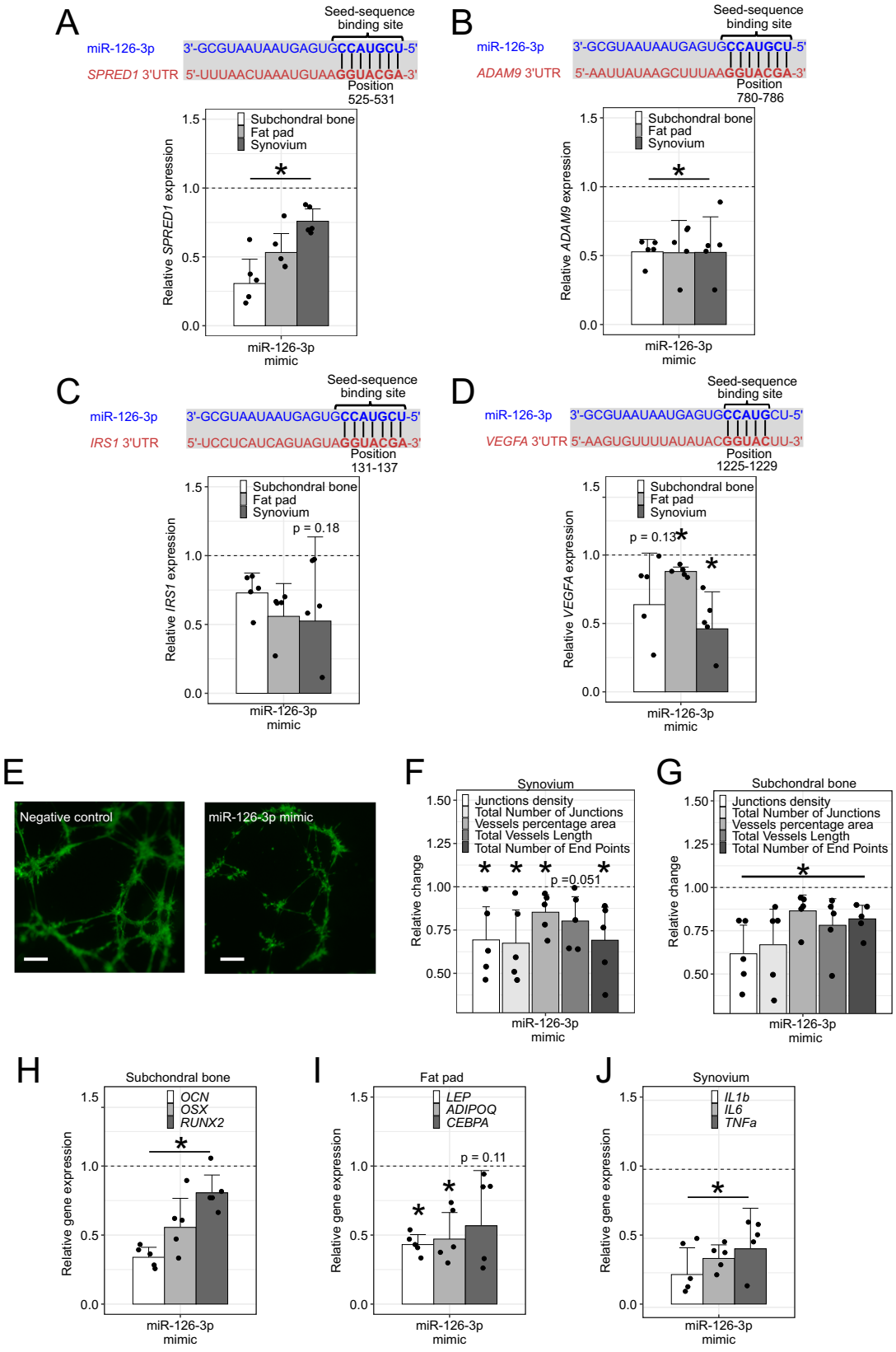

sequence binding), and therefore may be secondary effects of reduced angiogenesis[39,40,65]. Since angiogenesis increases in early stages of knee OA and is associated with worse outcomes[66,67], miR-126-3p may become elevated at KL ≥ 2 to regulate angiogenesis in a negative feedback mechanism. This may explain why we observed no effects of miR-126-3p in sham mice. At endogenous levels at KL ≥ 2, miR-126-3p may be insufficient to override pro-angiogenic signals, thus angiogenesis ensues and knee OA progresses. However, supplementing miR-126-3p levels bolsters its anti-angiogenic effects and improves knee OA outcomes in mice. Future dose-response experiments are required to define the optimal therapeutic range for mimic delivery and to assess potential effects on pain. Additional studies are also

https://doi.org/10.1038/s41467-025-57308-5

Fig. 5 | miR-126-3p shows anti-angiogenic effects in primary human knee OA tissues. A–D Seed sequence binding site locations and gene expression fold-changes in direct gene targets of miR-126-3p in knee OA tissue explants following transfection with miR-126-3p mimic ($n = 5$ biological replicates). **E** Representative images of primary human endothelial cells from knee OA subchondral bone stained with fluorescent dye to visualize 3D tube formation following transfection with miR-126-3p mimic. Scale bars = 200 μm. **F, G** Metrics associated with angiogenesis measured following transfection with miR-126-3p mimic in endothelial cells isolated from primary knee OA tissues ($n = 5$ biological replicates). **H–J** Gene expression fold-changes in knee OA subchondral bone, fat pad and synovium tissue explants following transfection with miR-126-3p mimic ($n = 5$ biological replicates). Data represented relative to negative control treated tissues/cells (dashed line, set to 1.0). Bars represent mean ± 95% confidence interval, $^*p < 0.05$ versus matched negative control. *SPRED1* sprouty related EVH1 domain containing 1, *ADAM9* a disintegrin and metalloproteinase domain 9, *IRS1* insulin receptor substrate 1, *VEGFA* vascular endothelial growth factor A, *OSX* osterix, *OCN* osteocalcin, *RUNX2* runt-related transcription factor 2, *CEBPA* CCAAT/enhancer-binding protein-alpha, *ADIPOQ* adiponectin, *LEP* leptin, *IL1b* interleukin 1 beta, *IL6* interleukin 6, *TNFa* tumor necrosis factor alpha. Source data are provided as a Source Data file. All statistical significance determined by paired two-sided Student's *t*-test. *P*-values: **A** $p = 0.007$ (subchondral bone), $p = 0.006$ (fat pad), $p = 0.008$ (synovium). **B** $p = 0.001$ (subchondral bone), $p = 0.026$ (fat pad), $p = 0.034$ (synovium). **C** $p = 0.026$ (subchondral bone), $p = 0.033$ (fat pad), $p = 0.177$ (synovium). **D** $p = 0.130$ (subchondral bone), $p = 0.002$ (fat pad), $p = 0.030$ (synovium). **F** $p = 0.035$ (junctions density), $p = 0.029$ (total number of junctions), $p = 0.046$ (vessels percentage area), $p = 0.051$ (total vessels length), $p = 0.034$ (total number of end points). **G** $p = 0.010$ (junctions density), $p = 0.034$ (total number of junctions), $p = 0.045$ (vessels percentage area), $p = 0.049$ (total vessels length), $p = 0.011$ (total number of end points). **H** $p = 0.000$ (*OCN*), $p = 0.023$ (*OSX*), $p = 0.047$ (*RUNX2*). **I** $p = 0.000$ (*LEP*), $p = 0.013$ (*ADIPOQ*), $p = 0.106$ (*CEPBA*). **J** $p = 0.009$ (*IL1b*), $p = 0.001$ (*IL6*), $p = 0.031$ (*TNFa*).

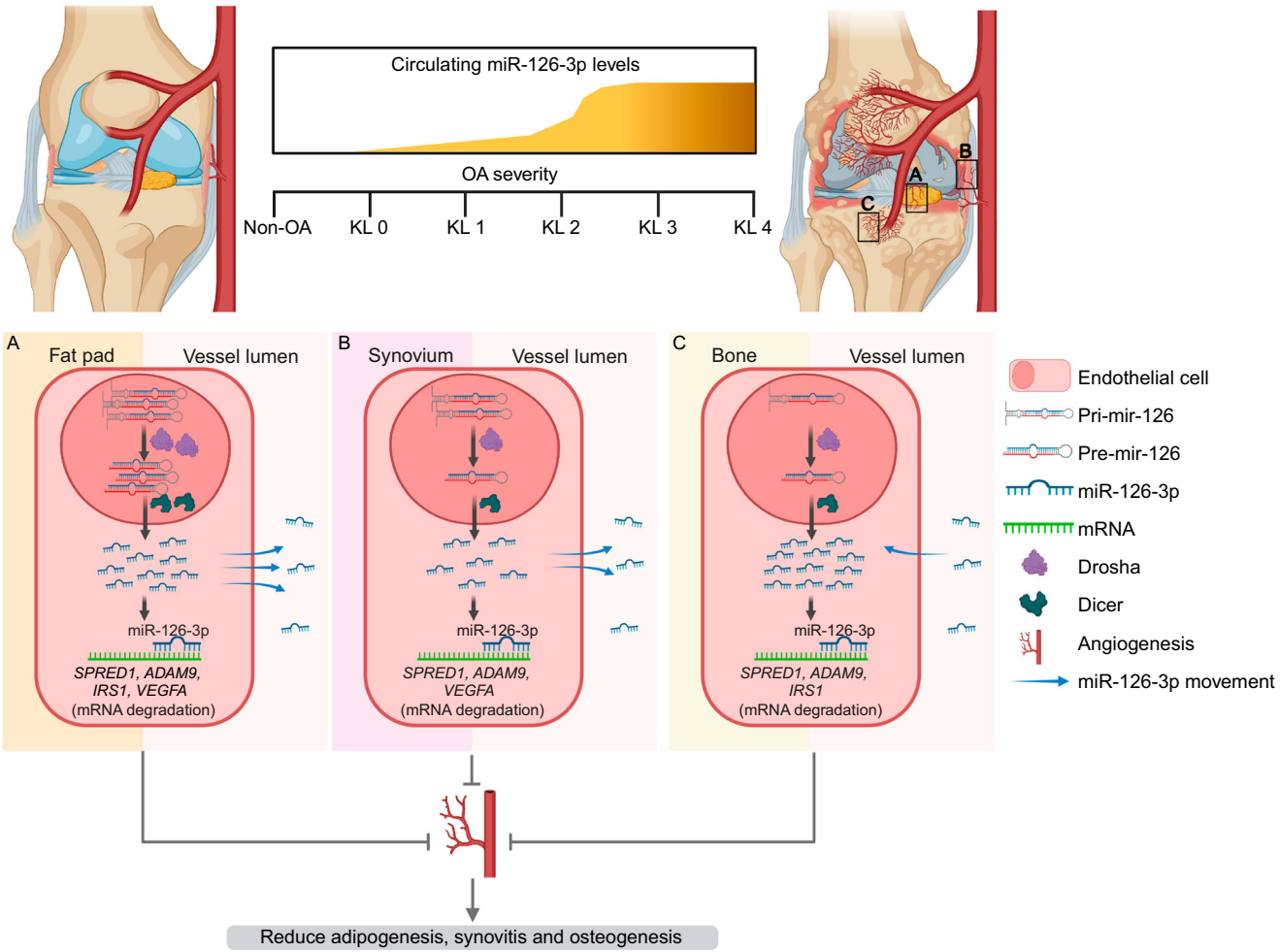

Fig. 6 | Proposed mechanism of action of miR-126-3p in knee OA. Our data suggest circulating levels of miR-126-3p become elevated in KL ≥ 2 knee OA via increased production and secretion by endothelial cells within the fat pad (**A**), and to a lesser extent, from the synovium (**B**). From circulation, miR-126-3p is then able to act distally, including in endothelial cells in the subchondral bone (**C**). Within each tissue, miR-126-3p regulates its direct gene targets including *SPRED1*, *ADAM9*, *IRS1*, and *VEGFA*, leading to a net reduction in angiogenesis. This anti-angiogenic effect in turn leads to secondary effects on adipogenesis in fat pad, synovitis in synovium, and osteogenesis in subchondral bone. Created in BioRender. Wilson, T. (2025) https://BioRender.com/d38r039.

required to assess joint-specific effects of miR-126-3p since our data show circulating levels are not elevated in hip OA, suggesting miR-126-3p-mediated mechanisms may be relevant to knee OA and not hip OA.

This study identifies a circulating microRNA that is consistently elevated in radiographic KL ≥ 2 knee OA versus non-OA individuals across four independent cohorts. We link circulating miR-126-3p to local knee tissues and show it exhibits a pro-resolving role in a surgical mouse model of knee OA. This effect is mediated at least in part by a reduction in angiogenesis, with secondary effects on osteogenesis, adipogenesis and synovitis. In sum, our findings suggest that miR-126-3p is a candidate mechanistic biomarker for radiographic knee OA that merits further investigation.

Methods

HFH OA cohort

All human biospecimens were obtained from our HFH OA Cohort ($N = 145$). OA participants included individuals undergoing total joint arthroplasty or arthroscopy for the treatment of symptomatic knee or hip OA as assessed by an orthopedic surgeon. Severity was determined using radiographic KL grade[22]. Non-OA control participants consisted of individuals with no radiographic evidence of knee or hip OA, including some individuals undergoing hip femoroplasty, acetabuloplasty or labral repair. All biospecimens were collected, processed and stored according to our previously published protocols[68]. Knee OA tissues included subchondral bone, infrapatellar fat pad, synovium, anterior cruciate ligament, meniscus and articular cartilage. Briefly, knee OA tissues were collected consistently by the same surgeons and dissected under sterile conditions within four hours of surgery, with subchondral bone and articular cartilage isolated from the anterior femoral condyle. Plasma was isolated from whole blood samples following centrifugation at 1700 × *g* for 10 min at 4 °C. Clinicodemographic data from each participant was captured and de-identified, including age, self-reported sex, BMI, race and comorbidities (Supplemental Table 1). As no significant relationship was identified between sex and miR-126-3p plasma levels, sex-specific differences were not assessed for the remainder of the study. The study protocol was approved by HFH Institutional Review Board (IRB #13995) and written informed consent was obtained from all participants prior to enrollment.

Primary tissue explants

Primary human knee OA tissue explants (~100 mg/well in a 24-well plate) were incubated in 500 μl Dulbecco's Modified Eagle's Medium (DMEM) supplemented with 1% penicillin-streptomycin (pen-strep) at 37 °C, with 5% CO_2. Secretion of microRNAs from knee OA tissue explants over time was assessed as outlined in Fig. 3H. Briefly, culture media were completely removed and replaced every 24 h, for a total of 72 h. The collected media samples were centrifuged at 10,000 × *g* for 5 min at 4 °C to pellet cellular debris with the supernatant collected and stored at −80 °C for further analysis.

MicroRNA mimic transfection

As human and mouse miR-126-3p is homologous, we used the same miR-126-3p oligonucleotides for microRNA modulation in our primary human OA tissue explants and knee OA mouse models. Primary human knee OA tissue explants (~ 100 mg/well in a 24-well plate) were cultured in 500 μl DMEM + 1% pen-strep. Tissues were transfected with 100 nM miRIDIAN microRNA Human hsa-miR-126-3p Mimic (designated as miR-126-3p mimic; Dharmacon) or 100 nM miRIDIAN microRNA Mimic Negative Control (designated as negative control; Dharmacon) in combination with 2.5 μl/well DharmaFECT-1 Transfection Reagent (Dharmacon) at 37 °C, as per the manufacturer's recommendations. This mimic serves as direct delivery of mature miR-126-3p sequences and does not alter endogenous production of miR-126-3p. After 24 h of incubation, tissues were collected, washed with sterile 1× phosphate buffered saline (PBS), flash frozen in liquid nitrogen and stored at −80 °C for subsequent analyses.

Surgical mouse model of knee OA

All animal experiments were approved by the HFH Institutional Animal Care and Use Committee (IACUC #1377). Eleven-week-old male C57BL/6J mice were purchased from Jackson Laboratories and acclimatized in-house for one week. Animals were housed under a 12-h light/dark cycle at 21 °C and 30% humidity. To minimize stress, animals were only handled by trained personnel during experimental procedures. All animals were monitored for adverse conditions by designated animal lab staff, with extra attention during the three-day post-operative period. No animals used in this study reached humane endpoint criteria. OA was induced via PMX, with the anterior half of the medial meniscus removed[26]. A concurrent group of mice were subjected to sham surgeries, with the medial meniscus left intact. We used only males as they display a more severe phenotype following surgical induction of OA. Four weeks following surgeries, mice were randomized into treatment groups ($N = 5$/group) consisting of miR-126-3p mimic (as described above), negative controls and miRIDIAN microRNA Human hsa-miR-126-3p Hairpin Inhibitor (designated as miR-126-3p inhibitor; Dharmacon). This inhibitor functions by binding to mature miR-126-3p sequences and blocking their activity. Treatments were given as weekly doses of 5 μg[17] (in 50 μL 1× PBS) via tail vein injections for a total of four treatments. This in vivo experimental model is outlined in Fig. 4A. A separate group of animals followed a similar experimental design, except that tail vein injections were replaced with IA injections (5 μg in 3 μL 1× PBS). For tail vein delivery, the negative control mimic and miRIDIAN microRNA Hairpin Inhibitor Negative Control (Dharmacon) treatments were combined (2.5 μg each in 1× PBS) and for IA delivery, the miR-126-3p inhibitor groups were excluded to reduce excess animal burden, in accordance with the three Rs ethical guiding principles of animal research[69]. At endpoint, animals were euthanized via carbon dioxide inhalation, with secondary assurance of death, and both hind limbs harvested. To assess the effects of knee OA on systemic miR-126-3p levels, blood samples were collected pre-surgery (12 weeks) and four weeks post-surgery (16 weeks). Plasma was isolated from whole blood samples following centrifugation at 1700 × *g* for 10 min at 4 °C.

RNA extraction and quality assessment

For plasma and tissue culture conditioned media, RNA was extracted using the miRNeasy Serum/Plasma Advanced Kit (QIAGEN, Inc.) according to the manufacturer's protocol. For tissue explants, RNA was isolated using our published protocols by phenol-chloroform extraction[68]. Briefly, after pulverization, tissues were lysed in TRIzol reagent (Invitrogen) for 30 min on ice and subjected to two rounds of chloroform extraction (10,000 × *g* for 12 min at 4 °C). RNA was precipitated with 100% isopropanol, then pelleted by centrifugation (12,000 × *g* for 25 min at 4 °C). RNA pellets were washed with ice-cold 75% ethanol three times, air dried, then eluted in 25 μl nuclease-free water. RNA concentration and quality were assessed using a NanoDrop 2000 spectrophotometer (Thermofisher Scientific).

Real-time polymerase chain reaction (RT-PCR)

For microRNA quantification, reverse transcription was performed using the TaqMan microRNA Reverse Transcription Kit and TaqMan microRNA Assays (Applied Biosystems), according to the manufacturer's instructions. For gene expression analysis, the High-Capacity cDNA Reverse Transcription kit (Applied Biosystems) was used to synthesize cDNA. RT-PCR was performed for both microRNA and genes using the QuantStudio 7 Pro Real-Time PCR System (Applied Biosystems) and TaqMan Gene Expression Assays (Applied Biosystems) or SYBR Green custom oligonucleotides (Sigma-Aldrich) as specified in Supplemental Table 2. *GAPDH* was used as the housekeeping gene for gene expression analyses and miR-24-3p as reference for microRNA quantification based on previous literature[17]. Results were analyzed using the delta-delta-Ct method[70].

Endothelial cell tube formation assay

Knee OA subchondral bone, fat pad and synovium explants were minced into small pieces (< $1mm^3$), washed with PBS and incubated for 45 minutes at 37 °C with 1 μg/ml collagenase type II solution (Worthington Biochemical). Primary endothelial cells were obtained following filtration through 70 μm cell strainers and centrifugation at 300 x *g* for 5 min. The pellet was resuspended, and the cells were cultured in endothelial cell medium (R&D Systems) to ~90–95%

confluence. Endothelial cell tube formation was assessed using an In Vitro Angiogenesis Assay Kit (Abcam). Briefly, extracellular matrix gel was added to 96-well plates and allowed to polymerize for 1 h. Approximately 10,000 cells were then added to each well in endothelial cell media transfected with 100 nM miR-126-3p mimic or negative control and incubated overnight at 37 °C and 5% CO_2. After incubation, the cells were washed and stained as per the manufacturer's instructions. Fluorescent images were captured using an Eclipse Ti-5 microscope (Nikon) and 3D tube formation variables were quantified using WimTube image analysis software (Onimagin Technologies).

Histological analyses

Harvested mouse knee joints were fixed in 10% neutral buffered formalin (NBF) at room temperature for 4 days and then decalcified using a 10% ethylenediaminetetraacetic acid (EDTA) solution (pH 7.6) at 4 °C with agitation for 21 days. Following embedding, 5-micron coronal sections were placed on charged slides, deparaffinized and stained with 0.1% Safranin-O solution to assess OA severity. Changes in cartilage were assessed according to the OARSI histopathology guidelines for mice[28]. Knee sections were divided into quadrants (medial femur, medial tibia, lateral femur, lateral tibia) and graded from 0 (no damage) to 6 (> 75% cartilage erosion) by three independent blinded observers. The maximum quadrant scores by each observer for each section were averaged. Synovitis was assessed by the Krenn scoring system[29]. Values of 0 (normal) to 3 (severe) were assigned for enlargement of the synovial lining, stroma cell density and infiltration of inflammatory cells, then summed. Total scores from each blinded observer were averaged. MiR-126-3p localization was assessed in human tissues by in situ hybridization[71]. Knee OA subchondral bone, infrapatellar fat pad and synovium explants were fixed for 4 days in 10% NBF, after which bone samples were decalcified using a 10% EDTA solution, as described above. Fixed tissues were embedded and sectioned at 2-micron thickness, and mounted on charged slides. MiR-126-3p was then visualized using the SR-hsa-miR-126-3p-S1 miRNAscope probe (Advanced Cell Diagnostics, Lot # 24291 A) with the RNAScope 2.5 HD kit (Advanced Cell Diagnostics), according to the manufacturer's instructions. Endothelial cells were marked by CD31 immunohistochemical staining. Tissues were fixed, decalcified and sectioned as described above. Sections were subjected to pretreatment with Tris-buffered saline/EDTA retrieval solution (pH 9.0) overnight at 56 °C. Slides were then rinsed, blocked for non-specific proteins and incubated overnight at 4 °C with anti-CD31 primary antibody (ab182981, Abcam, Lot # 1075935-1) at a 1:100 dilution. Stain detection was performed using horseradish peroxidase polymer and 3-amino-9-ethylcarbazole, followed by hematoxylin counterstaining. All stained slides were imaged using an Aperio ScanScope system (Leica Biosystems).

Statistics

All data analysis was performed using R statistical software (v. 4.4.0), individual R packages used are available upon request. All datapoints represent individual biological replicates. Unless otherwise noted, statistical significance was determined by the Mann–Whitney *U* test with Benjamini-Hochberg correction or one-way ANOVA followed by Dunnett's post hoc test for multiple comparisons and two-sided Student's *T*-test for single comparisons. Differential expression analysis of microRNA-sequencing datasets was performed on normalized counts using a quasi-likelihood negative binomial regression model with trended dispersion. We trained a random forest classification model and assessed discrimination performance by AUC analysis. Input data were randomly split into training (70%) and testing (30%) cohorts. Sensitivity and specificity values were determined at a cut-point of 50% probability. Statistical significance between AUCs was determined by the DeLong test[72]. Multiple linear regression was performed for covariate analysis. Relationships between plasma and tissue microRNA levels were assessed by Pearson correlation. A meta-analysis was performed using the R metafor package (v 4.6) with a random effects model to estimate the pooled effect size of miR-126-3p levels in radiographic knee OA across four cohorts. Effect sizes and variance within studies were calculated from raw data or estimated from *p*-values when no individual values were obtainable. Heterogeneity was assessed by intra-study variability (τ^2), Higgin's I^2 statistic and Cochran's *Q*-test[73].

Reporting summary

Further information on research design is available in the Nature Portfolio Reporting Summary linked to this article.

Data availability

Processed sequencing data from our secondary analysis are available on figshare (url: https://doi.org/10.6084/m9.figshare.25951270). The original sequencing data used in this manuscript were obtained upon request to the authors of two studies, Aae et al.[19] (https://doi.org/10.1016/j.ocarto.2019.100018) and Rousseau et al.[20] (https://doi.org/10.1186/s13075-019-2086-5). Source data are provided with this paper.

References

1. Collaborators GBDO. Global, regional, and national burden of osteoarthritis, 1990-2020 and projections to 2050: a systematic analysis for the Global Burden of Disease Study 2021. *Lancet Rheumatol.* **5**, e508–e522 (2023).
2. Buckwalter, J. A. & Mankin, H. J. Articular cartilage: degeneration and osteoarthritis, repair, regeneration, and transplantation. *Instr. Course Lect.* **47**, 487–504 (1998).
3. Loeser, R. F., Goldring, S. R., Scanzello, C. R. & Goldring, M. B. Osteoarthritis: a disease of the joint as an organ. *Arthritis Rheum.* **64**, 1697–1707 (2012).
4. Kolasinski, S. L. et al. 2019 American college of rheumatology/arthritis foundation guideline for the management of osteoarthritis of the hand, hip, and knee. *Arthritis Care Res.* **72**, 220–233 (2020).
5. Rocha, F. A. C. & Ali, S. A. Soluble biomarkers in osteoarthritis in 2022: year in review. *Osteoarthr. Cartil.* **31**, 167–176 (2023).
6. Mitchell, P. S. et al. Circulating microRNAs as stable blood-based markers for cancer detection. *Proc. Natl. Acad. Sci. USA* **105**, 10513–10518 (2008).
7. Ali, S. A. et al. Circulating microRNAs differentiate fast-progressing from slow-progressing and non-progressing knee osteoarthritis in the Osteoarthritis Initiative cohort. *Ther. Adv. Musculoskelet. Dis.* **14**, 1759720X221082917 (2022).
8. Guo, Z. et al. Genome-wide survey of tissue-specific microRNA and transcription factor regulatory networks in 12 tissues. *Sci. Rep.* **4**, 5150 (2014).
9. Endisha, H., Rockel, J., Jurisica, I. & Kapoor, M. The complex landscape of microRNAs in articular cartilage: biology, pathology, and therapeutic targets. *JCI Insight* **3**, e121630 (2018).
10. Kerschan-Schindl, K. et al. Diagnostic performance of a panel of miRNAs (OsteomiR) for osteoporosis in a cohort of postmenopausal women. *Calcif. Tissue Int.* **108**, 725–737 (2021).
11. Ali, S. A., Peffers, M. J., Ormseth, M. J., Jurisica, I. & Kapoor, M. The non-coding RNA interactome in joint health and disease. *Nat. Rev. Rheumatol.* **17**, 692–705 (2021).
12. O'Brien, J., Hayder, H., Zayed, Y. & Peng, C. Overview of MicroRNA biogenesis, mechanisms of actions, and circulation. *Front. Endocrinol. (Lausanne)* **9**, 402 (2018).
13. Hergenreider, E. et al. Atheroprotective communication between endothelial cells and smooth muscle cells through miRNAs. *Nat. Cell Biol.* **14**, 249–256 (2012).
14. Thomou, T. et al. Adipose-derived circulating miRNAs regulate gene expression in other tissues. *Nature* **542**, 450–455 (2017).

15. Vicente, R., Noel, D., Pers, Y. M., Apparailly, F. & Jorgensen, C. Deregulation and therapeutic potential of microRNAs in arthritic diseases. *Nat. Rev. Rheumatol.* **12**, 496 (2016).
16. Nakamura, A., Ali, S. A. & Kapoor, M. Antisense oligonucleotide-based therapies for the treatment of osteoarthritis: Opportunities and roadblocks. *Bone* **138**, 115461 (2020).
17. Endisha, H. et al. MicroRNA-34a-5p promotes joint destruction during osteoarthritis. *Arthritis Rheumatol.* **73**, 426–439 (2021).
18. Potla, P., Ali, S. A. & Kapoor, M. A bioinformatics approach to microRNA-sequencing analysis. *Osteoarthr. Cartil. Open* **3**, 100131 (2021).
19. Aae, T. F. K. T. A., Haugen, I. K., Risberg, M. A., Lian, Ø. B. & Brinchmann, J. E. Evaluating plasma extracellular vesicle microRNAs as possible biomarkers for osteoarthritis. *Osteoarthr. Cartil. Open* **1**, 100018 (2020).
20. Rousseau, J. C. et al. Association of circulating microRNAs with prevalent and incident knee osteoarthritis in women: the OFELY study. *Arthritis Res. Ther.* **22**, 2 (2020).
21. Ali, S. A. et al. Sequencing identifies a distinct signature of circulating microRNAs in early radiographic knee osteoarthritis. *Osteoarthritis Cartilage* **28**, 1471–1481 (2020).
22. Kellgren, J. H. & Lawrence, J. S. Radiological assessment of osteo-arthrosis. *Ann. Rheum. Dis.* **16**, 494–502 (1957).
23. Ameling, S. et al. Associations of circulating plasma microRNAs with age, body mass index and sex in a population-based study. *BMC Med. Genomics* **8**, 61 (2015).
24. Pereira, D. et al. Potential role of age, sex, body mass index and pain to identify patients with knee osteoarthritis. *Int. J. Rheum. Dis.* **20**, 190–198 (2017).
25. Borgonio Cuadra, V. M., Gonzalez-Huerta, N. C., Romero-Cordoba, S., Hidalgo-Miranda, A. & Miranda-Duarte, A. Altered expression of circulating microRNA in plasma of patients with primary osteoarthritis and in silico analysis of their pathways. *PLoS ONE* **9**, e97690 (2014).
26. Knights, C. B., Gentry, C. & Bevan, S. Partial medial meniscectomy produces osteoarthritis pain-related behaviour in female C57BL/6 mice. *Pain* **153**, 281–292 (2012).
27. Welch, I. D., Cowan, M. F., Beier, F. & Underhill, T. M. The retinoic acid binding protein CRABP2 is increased in murine models of degenerative joint disease. *Arthritis Res. Ther.* **11**, R14 (2009).
28. Glasson, S. S., Chambers, M. G., Van Den Berg, W. B. & Little, C. B. The OARSI histopathology initiative – recommendations for histological assessments of osteoarthritis in the mouse. *Osteoarthr. Cartil.* **18**, S17–S23 (2010).
29. Krenn, V. et al. Grading of chronic synovitis–a histopathological grading system for molecular and diagnostic pathology. *Pathol. Res. Pr.* **198**, 317–325 (2002).
30. Wang, S. et al. The endothelial-specific microRNA miR-126 governs vascular integrity and angiogenesis. *Dev. Cell* **15**, 261–271 (2008).
31. Jenike, A. E., Jenike, K. M., Peterson, K. J., Fromm, B. & Halushka, M. K. Direct observation of the evolution of cell-type-specific microRNA expression signatures supports the hematopoietic origin model of endothelial cells. *Evol. Dev.* **25**, 226–239 (2023).
32. Fish, J. E. et al. miR-126 regulates angiogenic signaling and vascular integrity. *Dev. Cell* **15**, 272–284 (2008).
33. Suresh Babu, S. et al. MicroRNA-126 overexpression rescues diabetes-induced impairment in efferocytosis of apoptotic cardiomyocytes. *Sci. Rep.* **6**, 36207 (2016).
34. Fang, S., Ma, X., Guo, S. & Lu, J. MicroRNA-126 inhibits cell viability and invasion in a diabetic retinopathy model via targeting IRS-1. *Oncol. Lett.* **14**, 4311–4318 (2017).
35. Chou, C. W., Huang, Y. K., Kuo, T. T., Liu, J. P. & Sher, Y. P. An overview of ADAM9: structure, activation, and regulation in human diseases. *Int. J. Mol. Sci.* **21**, 7790 (2020).
36. Katagiri, S. et al. Overexpressing IRS1 in endothelial cells enhances angioblast differentiation and wound healing in diabetes and insulin resistance. *Diabetes* **65**, 2760–2771 (2016).
37. Gondaliya, P., Driscoll, J., Yan, I. K., Ali Sayyed, A. & Patel, T. Therapeutic restoration of miR-126-3p as a multi-targeted strategy to modulate the liver tumor microenvironment. *Hepatol. Commun.* **8**, e0373 (2024).
38. Chen, H. et al. Reduced miR-126 expression facilitates angiogenesis of gastric cancer through its regulation on VEGF-A. *Oncotarget* **5**, 11873–11885 (2014).
39. Mapp, P. I. & Walsh, D. A. Mechanisms and targets of angiogenesis and nerve growth in osteoarthritis. *Nat. Rev. Rheumatol.* **8**, 390–398 (2012).
40. Cao, Y. Angiogenesis modulates adipogenesis and obesity. *J. Clin. Invest.* **117**, 2362–2368 (2007).
41. Donell, S. Subchondral bone remodelling in osteoarthritis. *EFORT Open Rev.* **4**, 221–229 (2019).
42. Collins, K. H. et al. Adipose tissue is a critical regulator of osteoarthritis. *Proc. Natl. Acad. Sci. USA* **118**, e2021096118 (2021).
43. Sanchez-Lopez, E., Coras, R., Torres, A., Lane, N. E. & Guma, M. Synovial inflammation in osteoarthritis progression. *Nat. Rev. Rheumatol.* **18**, 258–275 (2022).
44. Kohn, M. D., Sassoon, A. A. & Fernando, N. D. Classifications in Brief: Kellgren-Lawrence classification of osteoarthritis. *Clin. Orthop. Relat. Res.* **474**, 1886–1893 (2016).
45. Sapoval, M. et al. Genicular artery embolization for knee osteoarthritis: results of the LipioJoint-1 trial. *Diagn. Inter. Imaging* **105**, 144–150 (2024).
46. Landers, S. et al. Genicular artery embolization for early-stage knee osteoarthritis: results from a triple-blind single-centre randomized controlled trial. *Bone Jt. Open* **4**, 158–167 (2023).
47. Kok, M. G. M. et al. Small sample sizes in high-throughput miRNA screens: a common pitfall for the identification of miRNA biomarkers. *Biomol. Detect Quantif.* **15**, 1–5 (2018).
48. Cohen, J. F. et al. STARD 2015 guidelines for reporting diagnostic accuracy studies: explanation and elaboration. *BMJ Open* **6**, e012799 (2016).
49. Dong, Y. et al. Prognostic significance of miR-126 in various cancers: a meta-analysis. *Onco Targets Ther.* **9**, 2547–2555 (2016).
50. Balaskas, P. et al. MicroRNA profiling in cartilage ageing. *Int. J. Genomics* **2017**, 2713725 (2017).
51. Harris, T. A., Yamakuchi, M., Ferlito, M., Mendell, J. T. & Lowenstein, C. J. MicroRNA-126 regulates endothelial expression of vascular cell adhesion molecule 1. *Proc. Natl. Acad. Sci. USA* **105**, 1516–1521 (2008).
52. Hernandez, R., Orbay, H. & Cai, W. Molecular imaging strategies for in vivo tracking of microRNAs: a comprehensive review. *Curr. Med. Chem.* **20**, 3594–3603 (2013).
53. Zhou, Y. et al. Exosomes derived from miR-126-3p-overexpressing synovial fibroblasts suppress chondrocyte inflammation and cartilage degradation in a rat model of osteoarthritis. *Cell Death Discov.* **7**, 37 (2021).
54. Tuckermann, J. & Adams, R. H. The endothelium-bone axis in development, homeostasis and bone and joint disease. *Nat. Rev. Rheumatol.* **17**, 608–620 (2021).
55. Gu, Y. et al. Single-cell RNA sequencing in osteoarthritis. *Cell Prolif.* **56**, e13517 (2023).
56. Li, H. et al. Combining single-cell RNA sequencing and population-based studies reveals hand osteoarthritis-associated chondrocyte subpopulations and pathways. *Bone Res.* **11**, 58 (2023).
57. Jin, H. Y. et al. Transfection of microRNA mimics should be used with caution. *Front. Genet.* **6**, 340 (2015).
58. Gallant-Behm, C. L. et al. A microRNA-29 mimic (Remlarsen) represses extracellular matrix expression and fibroplasia in the skin. *J. Invest. Dermatol.* **139**, 1073–1081 (2019).

59. Reid, G. et al. Restoring expression of miR-16: a novel approach to therapy for malignant pleural mesothelioma. *Ann. Oncol.* **24**, 3128–3135 (2013).
60. Hong, D. S. et al. Phase 1 study of MRX34, a liposomal miR-34a mimic, in patients with advanced solid tumours. *Br. J. Cancer* **122**, 1630–1637 (2020).
61. Diener, C., Keller, A. & Meese, E. Emerging concepts of miRNA therapeutics: from cells to clinic. *Trends Genet.* **38**, 613–626 (2022).
62. Cao, D. et al. MicroRNA-126-3p inhibits angiogenic function of human lung microvascular endothelial cells via LAT1 (L-Type Amino Acid Transporter 1)-mediated mTOR (mammalian target of rapamycin) signaling. *Arterioscler Thromb. Vasc. Biol.* **40**, 1195–1206 (2020).
63. Tsumaru, S. et al. Therapeutic angiogenesis by local sustained release of microRNA-126 using poly lactic-co-glycolic acid nanoparticles in murine hindlimb ischemia. *J. Vasc. Surg.* **68**, 1209–1215 (2018).
64. Favero, M. et al. Infrapatellar fat pad features in osteoarthritis: a histopathological and molecular study. *Rheumatology* **56**, 1784–1793 (2017).
65. MacDonald, I. J. et al. Implications of angiogenesis involvement in arthritis. *Int. J. Mol. Sci.* **19**, 2012 (2018).
66. Su, W. et al. Angiogenesis stimulated by elevated PDGF-BB in subchondral bone contributes to osteoarthritis development. *JCI Insight* **5**, e135446 (2020).
67. Mapp, P. I. et al. Angiogenesis in two animal models of osteoarthritis. *Osteoarthr. Cartil.* **16**, 61–69 (2008).
68. Wilson, T., Kaur, N., Davis, J. & Ali, S. A. Tissue collection and RNA extraction from the human osteoarthritic knee joint. *J. Vis. Exp.* **173**, e62718 (2021).
69. Fenwick, N., Griffin, G. & Gauthier, C. The welfare of animals used in science: how the "Three Rs" ethic guides improvements. *Can. Vet. J.* **50**, 523–530 (2009).
70. Livak, K. J. & Schmittgen, T. D. Analysis of relative gene expression data using real-time quantitative PCR and the 2(-Delta Delta C(T)) method. *Methods* **25**, 402–408 (2001).
71. Endisha, H. & Kapoor, M. MicroRNA in situ hybridization in Paraffin-Embedded human articular cartilage and mouse knee joints. *Methods Mol. Biol.* **2245**, 93–103 (2021).
72. DeLong, E. R., DeLong, D. M. & Clarke-Pearson, D. L. Comparing the areas under two or more correlated receiver operating characteristic curves: a nonparametric approach. *Biometrics* **44**, 837–845 (1988).
73. Higgins, J. P. & Thompson, S. G. Quantifying heterogeneity in a meta-analysis. *Stat. Med.* **21**, 1539–1558 (2002).

Acknowledgements

This study was funded in part by a grant awarded to S.A.A. from the Arthritis National Research Foundation (ANRF 953971). We thank the authors of the original sequencing papers (Aae et al.[19] and Rousseau et al.[20]) for providing raw sequencing data. We also thank participants of the Henry Ford Health OA Cohort for donating biospecimens. We appreciate support from the William Clay Ford Chair at the Department of Orthopedics Henry Ford Health.

Author contributions

T.G.W., M.B., and S.A.A. were involved in study conception and design. T.G.W., M.B., and N.K. performed experimental work and data acquisition. P.P., I.D., and I.L. were involved in secondary analysis of the sequencing datasets. L.H., D.M., K.B., T.S.L., V.M., and J.D. contributed to the HFH OA Cohort biospecimens and data. T.G.W., M.B., and S.A.A. performed data analysis, interpretation and drafted the manuscript. All authors contributed to manuscript revisions and approved the final version.

Competing interests

The authors declare no competing interests.

Additional information

Supplementary information The online version contains supplementary material available at https://doi.org/10.1038/s41467-025-57308-5.

Correspondence and requests for materials should be addressed to Shabana Amanda Ali.

Peer review information *Nature Communications* thanks Danny Chan and Bastian Fromm for their contribution to the peer review of this work. A peer review file is available.